# Neutrinoless double-β decay matrix elements in light nuclei

S. Pastore, J. Carlson, V. Cirigliano, W. Dekens, E. Mereghetti, and R. B. Wiringa

# Neutrinoless double beta decay matrix elements in light nuclei

S. Pastore[a], J. Carlson [a], V. Cirigliano[a], W. Dekens[a,b], E. Mereghetti[a], and R.B. Wiringa[c]

[a] Theoretical Division, Los Alamos National Laboratory, Los Alamos, NM 87545
[b] New Mexico Consortium, Los Alamos Research Park, Los Alamos, NM 87544, USA
[c] Physics Division, Argonne National Laboratory, Argonne, IL 60439

We present the first *ab initio* calculations of neutrinoless double beta decay matrix elements in $A = 6$–12 nuclei using Variational Monte Carlo wave functions obtained from the Argonne $v_{18}$ two-nucleon potential and Illinois-7 three-nucleon interaction. We study both light Majorana neutrino exchange and potentials arising from a large class of multi-TeV mechanisms of lepton number violation. Our results provide benchmarks to be used in testing many-body methods that can be extended to the heavy nuclei of experimental interest. In light nuclei we have also studied the impact of two-body short range correlations and the use of different forms for the transition operators, such as those corresponding to different orders in chiral effective theory.

## I. INTRODUCTION

Searches for neutrinoless double beta decay $(0\nu\beta\beta)$ constitute the most sensitive laboratory probe of lepton number violation (LNV). In $0\nu\beta\beta$ two neutrons in a nucleus turn into two protons, with the emission of two electrons and no neutrinos, violating $L$ by two units. The observation of $0\nu\beta\beta$ would demonstrate that neutrinos are Majorana fermions [1], shed light on the mechanism of neutrino mass generation, and give insight into leptogenesis scenarios for the generation of the matter-antimatter asymmetry in the universe [2].

For certain even-even nuclei the single $\beta$ decay is energetically forbidden. In many such nuclei, the Standard Model allowed two-neutrino double beta decay has already been observed [3–8] (see Ref. [9] for older references), and the search for the LNV neutrinoless mode is being pursued by many collaborations worldwide. The current experimental limits on the half-lives for the neutrinoless mode are quite impressive [10–17], at the level of $T_{1/2} > 5.3 \times 10^{25}$ y for $^{76}$Ge [17] and $T_{1/2} > 1.07 \times 10^{26}$ y for $^{136}$Xe [10], with next generation ton-scale experiments aiming at two orders of magnitude sensitivity improvements.

The observation of $0\nu\beta\beta$, while of great significance by itself, would not immediately point to the underlying mechanism of lepton number violation. In fact, next-generation experiments are sensitive to a variety of mechanisms, which are most efficiently discussed in an effective theory approach to new physics, in which LNV arises from $\Delta L = 2$ operators of odd dimension, starting at dimension-five [18–21]. As discussed for example in Ref. [22], if the scale of lepton number violation, $\Lambda_{\mathrm{LNV}}$ is in the range 1-100 TeV, short-distance effects encoded in local operators of dimension seven and nine provide contributions to $0\nu\beta\beta$ within reach of next generation experiments. On the other hand, whenever $\Lambda_{\mathrm{LNV}}$ is much higher than the TeV scale, the only low-energy manifestation of this new physics is a Majorana mass for light neutrinos, encoded in a single gauge-invariant dimension-five operator [18], which induces $0\nu\beta\beta$ through light Majorana-neutrino exchange [23, 24].

To interpret positive or null $0\nu\beta\beta$ results in the context of various LNV mechanisms it is essential to have control over the relevant hadronic and nuclear matrix elements. Current knowledge of these is somewhat unsatisfactory [25], as various many-body approaches lead to estimates that differ by a factor of two to three for nuclei of experimental interest. This is true both for the light Majorana-neutrino exchange mechanism, which has received much attention in the literature, and for short-distance sources of LNV encoded in dimension-seven and -nine operators (see [22] and references therein).

In this paper we present the first *ab initio* calculations of $0\nu\beta\beta$ nuclear matrix elements in light nuclei ($A = 6$–12), using Variational Monte Carlo (VMC) wave functions obtained from the Argonne $v_{18}$ (AV18) [26] two-body potential and Illinois-7 (IL7) [27] three-nucleon interaction. We use the measured value of the axial coupling constant $g_A = 1.2723(23)$ [28]—also utilized in recent *ab initio* quantum Monte Carlo calculations of single beta decays in $A = 6$–10 nuclei [29] that explain the data at the $\leq 2\%$ ($\sim 10\%$) level in $A = 6$–7 ($A = 10$) decays—and compare with results for $A = 48$–136 nuclei [30, 31] also based on the measured value of $g_A$. We study the matrix elements of light Majorana-neutrino exchange as well as those arising from a large class of multi-TeV mechanisms of LNV. While the transitions studied here are not directly relevant from an experimental point of view, this study has several merits: (i) Because the *ab initio* framework used here accurately explains, qualitatively and quantitatively, the observed properties of light nuclei [32–34], our results provide an important benchmark to test other many-body methods that can be extended to the heavy nuclei of experimental interest. (ii) In this framework we can study in a controlled way the impact of various approximations inherent to some many-body methods – such as neglecting two body correlations. (iii) For a given LNV mechanism, we can explore the impact of using different forms for the transition operators ("po-

tentials") mediating $0\nu\beta\beta$. (iv) In the same vein, we can study the relative size of matrix elements corresponding to different LNV mechanisms.

The paper is organized as follows. In Section II we present the two-body transition operators ("potentials") that mediate $0\nu\beta\beta$ from a large class of LNV mechanisms. In Section III we describe the VMC method and in Section IV we discuss our results. We present our conclusions in Section V and provide some details on the potentials in coordinate space in Appendix A.
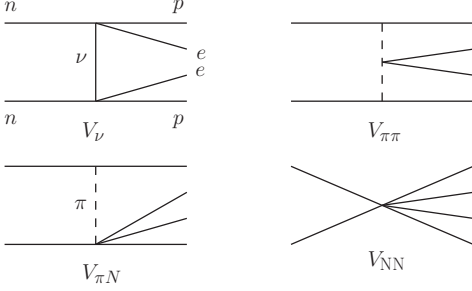


FIG. 1. Diagrams illustrating the $0\nu\beta\beta$ potentials mediated by neutrinos—$V_\nu$ defined in Eq. (6)—and two-pion-exchange, one-pion-exchange, and short-distance interactions—$V_{\pi\pi}$, $V_{\pi N}$, and $V_{NN}$ defined in Eqs. (12).

## II. NUCLEAR OPERATORS FOR $0\nu\beta\beta$

### A. Matching quark operators to hadronic operators

Our starting point is a $\Delta L = 2$ effective Lagrangian $\mathcal{L}_{\Delta L=2}$ at the hadronic scale $E \sim \Lambda_\chi \sim$ GeV written in terms of leptons and quarks. This effective Lagrangian originates from integrating out heavy new physics at the scale $\Lambda_{\text{LNV}}$ and matching onto $SU(3)_C \times SU(2)_L \times U(1)_Y$-invariant operators. After integrating out the heavy SM fields at the electroweak scale, one obtains a set of $SU(3)_C \times U(1)_{\text{EM}}$-invariant operators that we incorporate into our effective Lagrangian. In this work, with the purpose of benchmarking nuclear matrix elements, we include only the Majorana neutrino mass operator, which

is dimension three after electroweak symmetry breaking, and a subset of dimension-nine six-fermion operators that mediate short-range contributions to $0\nu\beta\beta$:

$$\mathcal{L}_{\Delta L=2} = -\frac{1}{2} m_{\beta\beta} \, \nu_{eL}^T C \nu_{eL} + \mathcal{L}_{\Delta L=2}^{(9)} + \text{h.c.} \, , \quad (1)$$

$$\mathcal{L}_{\Delta L=2}^{(9)} = \frac{V_{ud}^2}{v^5} \times \bar{e}_L C \bar{e}_L^T \left\{ C_1^{(9)} \, \bar{u}_L \gamma^\mu d_L \, \bar{u}_L \gamma_\mu d_L \right. \quad (2)$$
$$+ C_2^{(9)} \, \bar{u}_L d_R \, \bar{u}_L d_R + C_3^{(9)} \, \bar{u}_L^\alpha d_R^\beta \, \bar{u}_L^\beta d_R^\alpha$$
$$\left. + C_4^{(9)} \, \bar{u}_L \gamma^\mu d_L \, \bar{u}_R \gamma_\mu d_R + C_5^{(9)} \, \bar{u}_L^\alpha \gamma^\mu d_L^\beta \, \bar{u}_R^\beta \gamma_\mu d_R^\alpha \right\} \, .$$

Here $v = (\sqrt{2} G_F)^{-1/2} = 246$ GeV, $\alpha$, $\beta$ are color indices, and for later convenience we have extracted a factor of $V_{ud}^2$ from the dimensionless Wilson coefficients $C_i^{(9)}$. The dimension-three term in Eq. (1) originates from the only $SU(2)_L$-invariant operator at dimension-five, while the dimension-nine terms can arise from both dimension-seven and -nine $SU(2)_L$-invariant operators.

In principle, the most general $\Delta L = 2$ low-energy effective Lagrangian would include additional dimension-six and -seven charged-current operators, which give rise to long-range contributions to $0\nu\beta\beta$, not proportional to $m_{\beta\beta}$. However, as was shown in Ref. [22], the nuclear matrix elements (NMEs) needed in this case are related to NMEs that appear in light and heavy Majorana-neutrino exchange, and thus do not require independent calculations. Furthermore, the effective Lagrangian in (2) represents a subset of the most general dimension-nine $\Delta L = 2$ interactions. The complete basis of dimension-nine operators includes additional terms that can be obtained by the interchange of $L \leftrightarrow R$ on the quark and/or lepton-fields in (2), as well as operators in which the quark and electron structures are Lorentz vectors (e.g. $\bar{e}_L \gamma_\mu C \bar{e}_R^T$) [35, 36]. However, as far as $0^+ \to 0^+$ transitions are concerned, none of these additional operators lead to different hadronic realizations than those induced by the operators in Eq. (2) [37]. As a result, the NMEs studied in the following capture the leading contributions to $0\nu\beta\beta$ from $SU(2)_L$-invariant operators of dimension-five and -seven, as well as those from dimension-nine operators involving six fermions.

The leading low-energy realization of the effective Lagrangian (1) in terms of leptons, pions, and nucleons, reads [36, 37]

$$\mathcal{L}_{\Delta L=2} = -\frac{1}{2} m_{\beta\beta} \, \nu_{eL}^T C \nu_{eL} + \frac{V_{ud}^2}{v^5} \times \bar{e}_L C \bar{e}_L^T \left\{ \frac{5}{6} C_1^{(9)} \, g_{27\times 1} F_\pi^2 \partial_\mu \pi^- \partial^\mu \pi^- \right.$$
$$+ \frac{1}{2} F_\pi^2 \left( C_4^{(9)} g_{8\times 8} + C_5^{(9)} g_{8\times 8}^{\text{mix}} - C_2^{(9)} g_{6\times 6} - C_3^{(9)} g_{6\times\bar{6}}^{\text{mix}} \right) \pi^- \pi^-$$
$$\left. + \sqrt{2} g_A F_\pi C_1^{(9)} \, g_{27\times 1}^{\pi N} \, \bar{p} S \cdot (\partial \pi^-) n + \frac{1}{2} C_1^{(9)} g_{27\times 1}^{NN} \, \bar{p} n \bar{p} n \right\} \, . \quad (3)$$

The low-energy constants (LECs) $g_{8\times 8}$ and $g_{6\times\bar{6}}$ are of $\mathcal{O}(\Lambda_\chi^2)$, while $g_{27\times 1}$ and $g_{27\times 1}^{\pi N}$ are of $\mathcal{O}(1)$. The coupling

constant of the $\Delta L = 2$ four-nucleon operator, $g_{27\times1}^{NN}$, is $\mathcal{O}(1)$ in the Weinberg power counting [38, 39]. We follow the notation of Ref. [37], in which $g_{8\times8}$, $g_{6\times\bar{6}}$, and $g_{27\times1}$ (see also Ref. [40]) were estimated using $SU(3)$ chiral perturbation theory ($\chi$PT) relations and lattice-QCD calculations of kaon matrix elements. At $\mu = 3$ GeV in the $\overline{\text{MS}}$ scheme one has $g_{27\times1} = 0.37 \pm 0.08$, $g_{8\times8} = -(3.1 \pm 1.3)$ GeV$^2$, $g_{8\times8}^{\text{mix}} = -(13 \pm 4)$ GeV$^2$, $g_{6\times\bar{6}} = (3.2 \pm 0.7)$ GeV$^2$, $g_{6\times\bar{6}}^{\text{mix}} = -(1.1 \pm 0.3)$ GeV$^2$. For the new-physics operators that transform as $8_L \times 8_R$ or $6_L \times \bar{6}_R$, within the Weinberg power counting, only the $\pi\pi$ interactions contribute at LO, and we neglect the subleading pion-nucleon and nucleon-nucleon couplings in Eq. (3). Instead, for the operator transforming as $27_L \times 1_R$, we include all three types of interactions as they contribute to $0\nu\beta\beta$ at the same order.

### B. The isotensor nuclear potentials

From the effective Lagrangian (3) one obtains the following $\Delta L = 2$ effective hamiltonian for $0\nu\beta\beta$ in terms of electrons and nucleons:

$$H_{\Delta L=2} = 2G_F^2 V_{ud}^2\, \bar{e}_L C \bar{e}_L^T \sum_{a,b} V(a,b)\,, \qquad (4)$$

with the isotensor potential given by

$$V = m_{\beta\beta} V_\nu + \frac{m_\pi^2}{v}\left(c_{\pi\pi} V_{\pi\pi} + c_{\pi N} V_{\pi N} + c_{NN} V_{NN}\right).(5)$$

In what follows we will give the two-body potentials in momentum space, while providing their coordinate space expressions in Appendix A.

#### 1. Light Majorana neutrino exchange

The first term in Eq. (5) is generated by light Majorana-neutrino exchange, depicted in the top-left panel of Fig. 1, and at leading order is given by

$$V_\nu = \tau_a^+ \tau_b^+ \frac{1}{\mathbf{q}^2}\left\{ g_V^2 \right.$$
$$- g_A^2\left[\boldsymbol{\sigma}_a \cdot \boldsymbol{\sigma}_b \left(1 - \frac{2}{3}\frac{\mathbf{q}^2}{\mathbf{q}^2 + m_\pi^2} + \frac{1}{3}\frac{(\mathbf{q}^2)^2}{(\mathbf{q}^2 + m_\pi^2)^2}\right)\right.$$
$$\left.\left. - \frac{S_{ab}(\hat{\mathbf{q}})}{3}\left(-\frac{2\mathbf{q}^2}{\mathbf{q}^2 + m_\pi^2} + \frac{(\mathbf{q}^2)^2}{(\mathbf{q}^2 + m_\pi^2)^2}\right)\right]\right\}, \quad (6)$$

where $\hat{\mathbf{q}} = \mathbf{q}/|\mathbf{q}|$, $g_V = 1$, $g_A = 1.27$, and the tensor operator is given by $S_{ab} = -\left(3\boldsymbol{\sigma}_a \cdot \hat{\mathbf{q}}\,\boldsymbol{\sigma}_b \cdot \hat{\mathbf{q}} - \boldsymbol{\sigma}_a \cdot \boldsymbol{\sigma}_b\right)$ in momentum space. Higher-order corrections to the single-nucleon charged-currents can be taken into account by including momentum-dependent form factors and contributions proportional to the nucleon isovector magnetic moment. These effects appear at N$^2$LO in the chiral

power counting, while two-body effects in the weak currents [41–43], which induce three-nucleon potentials, appear at N$^3$LO. Here we parametrize the N$^2$LO terms by following Ref. [25] and re-expressing $V_\nu$ as

$$V_\nu = \tau_a^+ \tau_b^+ \frac{g_A^2}{\mathbf{q}^2}\left\{\frac{g_V^2}{g_A^2}v_F^\nu(\mathbf{q}^2)\right.$$
$$\left. - \boldsymbol{\sigma}_a \cdot \boldsymbol{\sigma}_b\, v_{GT}^\nu(\mathbf{q}^2) - S_{ab}\, v_T^\nu(\mathbf{q}^2)\right\}. \qquad (7)$$

The Fermi (F), Gamow-Teller (GT) and tensor (T) functions can be expressed in terms of the nucleon isovector vector, axial, induced pseudoscalar and tensor form factors as

$$v_F^\nu(\mathbf{q}^2) = g_V^2(\mathbf{q}^2)/g_V^2\,,$$
$$v_{GT}^\nu(\mathbf{q}^2) = v_{GT}^{AA}(\mathbf{q}^2) + v_{GT}^{AP}(\mathbf{q}^2) + v_{GT}^{PP}(\mathbf{q}^2) + v_{GT}^{MM}(\mathbf{q}^2)\,,$$
$$v_T^\nu(\mathbf{q}^2) = v_T^{AP}(\mathbf{q}^2) + v_T^{PP}(\mathbf{q}^2) + v_T^{MM}(\mathbf{q}^2)\,, \qquad (8)$$

where for the GT and T terms we have

$$v_{GT,T}^{AA}(\mathbf{q}^2) = \frac{g_A^2(\mathbf{q}^2)}{g_A^2}\,,$$
$$v_{GT}^{AP}(\mathbf{q}^2) = \frac{g_P(\mathbf{q}^2)}{g_A^2}\, g_A(\mathbf{q}^2)\frac{\mathbf{q}^2}{3m_N}\,,$$
$$v_{GT}^{PP}(\mathbf{q}^2) = \frac{g_P^2(\mathbf{q}^2)}{g_A^2}\frac{\mathbf{q}^4}{12m_N^2}\,,$$
$$v_{GT}^{MM}(\mathbf{q}^2) = g_M^2(\mathbf{q}^2)\frac{\mathbf{q}^2}{6g_A^2 m_N^2}\,, \qquad (9)$$

and $v_T^{AP}(\mathbf{q}^2) = -v_{GT}^{AP}(\mathbf{q}^2)$, $v_T^{PP}(\mathbf{q}^2) = -v_{GT}^{PP}(\mathbf{q}^2)$, and $v_T^{MM}(\mathbf{q}^2) = v_{GT}^{MM}(\mathbf{q}^2)/2$.

As commonly done in the $0\nu\beta\beta$ literature, we use a dipole parameterization for the vector and axial form factors, and write

$$g_V(\mathbf{q}^2) = g_V\left(1 + \frac{\mathbf{q}^2}{\Lambda_V^2}\right)^{-2}\,, \quad g_M(\mathbf{q}^2) = (1 + \kappa_1)g_V(\mathbf{q}^2)\,,$$
$$g_A(\mathbf{q}^2) = g_A\left(1 + \frac{\mathbf{q}^2}{\Lambda_A^2}\right)^{-2}\,, \quad g_P(\mathbf{q}^2) = -\frac{2m_N g_A(\mathbf{q}^2)}{\mathbf{q}^2 + m_\pi^2}, \quad (10)$$

where the vector and axial masses are $\Lambda_V = 850$ MeV and $\Lambda_A = 1040$ MeV, and the anomalous nucleon isovector magnetic moment $\kappa_1 = 3.7$. In the limit $\Lambda_{A,V} \to \infty$, Eq. (10) reduces to the leading order (LO) $\chi$PT expression. In what follows, we define the neutrino potentials in momentum space as

$$V_{\alpha,\beta}(\mathbf{q}^2) = \frac{1}{\mathbf{q}^2}v_\alpha^\beta(\mathbf{q}^2)\,, \qquad (11)$$

with $\alpha \in \{F, GT, T\}$ and $\beta \in \{\nu, AA, AP, PP, MM\}$, and the functions $v_\alpha^\beta$ given in Eqs. (8) and (9). The potential $V_{T,AA}$ does not appear in the case of light Majorana-neutrino exchange, but it is relevant in the presence of right-handed charged-currents [22, 44, 45]

Additional non-factorizable contributions to $V_\nu$ arise at the same order as form-factor corrections, as recently shown in Ref. [46]. We explore the impact of these in Section. IV D.

### 2. LNV from short-distance

The dimension-nine operators with couplings $C_i^{(9)}$ induce the pion-range and short-range potentials $V_{\pi\pi}$, $V_{\pi N}$ and $V_{NN}$ in Eq. (5) through the diagrams shown in Fig. 1:

$$V_{\pi\pi} = \tau_a^+\tau_b^+ (\boldsymbol{\sigma}_a \cdot \boldsymbol{\sigma}_b - S_{ab}) \frac{\mathbf{q}^2}{3(\mathbf{q}^2 + m_\pi^2)^2} ,$$

$$V_{\pi N} = -\tau_a^+\tau_b^+ \left(\boldsymbol{\sigma}_a \cdot \boldsymbol{\sigma}_b + S_{ab}\frac{\mathbf{q}^2}{m_\pi^2}\right) \frac{1}{3(\mathbf{q}^2 + m_\pi^2)} ,$$

$$V_{NN} = \tau_a^+\tau_b^+ \frac{1}{m_\pi^2} , \tag{12}$$

where we eliminated a GT-like contact interaction by use of the Fierz relation, $(\bar{p}\boldsymbol{\sigma}n)(\bar{p}\boldsymbol{\sigma}n) = -3(\bar{p}n)(\bar{p}n)$. As for the light Majorana-neutrino exchange potential $V_\nu$, we split the $V_{\pi\pi}$ and $V_{\pi N}$ in Gamow-Teller and tensor components (see Appendix A). The dimensionless effective couplings are given by:

$$c_{\pi\pi} = -\frac{g_A^2}{2m_\pi^2}\Big(C_4^{(9)}g_{8\times8} + C_5^{(9)}g_{8\times8}^{\text{mix}} - C_2^{(9)}g_{6\times6}$$
$$- C_3^{(9)}g_{6\times6}^{\text{mix}} + \frac{5}{3}C_1^{(9)}g_{27\times1}m_\pi^2\Big) , \tag{13}$$

$$c_{\pi N} = -g_A^2 C_1^{(9)}\left(g_{27\times1}^{\pi N} - \frac{5}{6}g_{27\times1}\right) , \tag{14}$$

$$c_{NN} = -C_1^{(9)}\left(g_{27\times1}^{NN} - g_A^2\left(g_{27\times1}^{\pi N} - \frac{5}{6}g_{27\times1}\right)\right) \tag{15}$$

At leading order in chiral EFT, the potentials in Eq. (12) do not include momentum dependent form factors. Note that, after absorbing the short-distance pieces of the $c_{\pi N}$ and $c_{\pi\pi}$ contributions into $V_{NN}$, we have $V_{GT,\pi\pi} = -V_{GT,PP}$ and $V_{GT,\pi N} = -V_{GT,AP}/2$ (see Appendix A). In our analysis, we will study the sensitivity to the large momentum region by multiplying $V_{\pi\pi}$, $V_{\pi N}$ and $V_{NN}$ by a dipole form factor, for which we take $g_A^2(\mathbf{q}^2)/g_A^2$.

### C. Matrix elements

To make contact with the standard $0\nu\beta\beta$ literature, it is convenient to define the dimensionless matrix elements between the initial and final nuclear states, $|\Psi_i\rangle$ and $|\Psi_f\rangle$, as

$$M^{\alpha,\beta} = \langle\Psi_f|O^{\alpha,\beta}|\Psi_i\rangle , \tag{16}$$

where the two-body F, GT, and T operators are given by

$$O^{F,\beta} = (4\pi R_A)\sum_{a,b} V_{F,\beta}(r_{ab})\,\tau_a^+\tau_b^+ , \tag{17}$$

$$O^{GT,\beta} = (4\pi R_A)\sum_{a,b} V_{GT,\beta}(r_{ab})\,\boldsymbol{\sigma}_a\cdot\boldsymbol{\sigma}_b\,\tau_a^+\tau_b^+ , \tag{18}$$

$$O^{T,\beta} = (4\pi R_A)\sum_{a,b} V_{T,\beta}(r_{ab})\,S_{ab}\,\tau_a^+\tau_b^+ , \tag{19}$$

where $R_A = 1.2\,A^{1/3}$ fm is the nuclear radius and now $\beta \in \{\nu, AA, AP, PP, MM, \pi\pi, \pi N, NN\}$. Note that the operators defined above involve an unconstrained sum over $a \neq b$. The potentials in momentum and coordinate space are related by

$$V_{\alpha,\beta}(r_{ab}) = \int \frac{d^3q}{(2\pi)^3} e^{i\mathbf{q}\cdot\mathbf{r}_{ab}}\, V_{\alpha,\beta}(\mathbf{q}). \tag{20}$$

For completeness, we report explicit expressions for the potentials in coordinate space in Appendix A.

## III. VARIATIONAL MONTE CARLO METHOD

The evaluation of the matrix elements defined in Eq. (16) is carried out using Variational Monte Carlo (VMC) computational algorithms [32]. The VMC wave function $\Psi(J^\pi; T, T_z)$—where $J^\pi$ and $T$ are the spin-parity and isospin of the state—is constructed from products of two- and three-body correlation operators acting on an antisymmetric single-particle state of the appropriate quantum numbers. The correlation operators are designed to reflect the influence of the two- and three-body nuclear interactions at short distances, while appropriate boundary conditions are imposed at long range [47, 48].

The $\Psi(J^\pi; T, T_z)$ has embedded variational parameters that are adjusted to minimize the expectation value

$$E_V = \frac{\langle\Psi|H|\Psi\rangle}{\langle\Psi|\Psi\rangle} \geq E_0 , \tag{21}$$

which is evaluated by Metropolis Monte Carlo integration [49]. In the equation above, $E_0$ is the exact lowest eigenvalue of the nuclear Hamiltonian $H$ for the specified quantum numbers. The many-body Hamiltonian is given by

$$H = \sum_i K_i + \sum_{i<j} v_{ij} + \sum_{i<j<k} V_{ijk} , \tag{22}$$

where $K_i$ is the non-relativistic kinetic energy of nucleon $i$ and $v_{ij}$ and $V_{ijk}$ are, respectively, the Argonne $v_{18}$ (AV18) [26] two-body potential and the Illinois-7 (IL7) [27] three-nucleon interaction. The AV18+IL7 model reproduces the experimental binding energies, charge radii, electroweak transitions and responses of $A = 3$–12 systems in numerically exact calculations based on Green's function Monte Carlo (GFMC) methods [29, 32–34].

A good variational wave function, that serves as the starting point of GFMC calculations, can be constructed with

$$|\Psi_V\rangle = \mathcal{S}\prod_{i<j}^A\left[1 + U_{ij} + \sum_{k\neq i,j}^A \tilde{U}_{ijk}\right]|\Psi_J\rangle. \tag{23}$$

The Jastrow wave function $\Psi_J$ is fully antisymmetric, translationally invariant, has the $(J^\pi; T, T_z)$ quantum

numbers of the state of interest, and includes a product over pairs of a central correlation function $f(r_{ij})$ that is small at short distances, peaks around 1 fm, and decays exponentially at long range [50]. The $U_{ij}$ and $\tilde{U}_{ijk}$ are the two- and three-body correlation operators, and $\mathcal{S}$ is a symmetrization operator. The two-body correlation operators [32, 50] can be schematically written as

$$U_{ij} = \sum_p f^p(r_{ij}) O_{ij}^p , \qquad (24)$$

where

$$O_{ij}^p = \boldsymbol{\tau}_i \cdot \boldsymbol{\tau}_j , \, \boldsymbol{\sigma}_i \cdot \boldsymbol{\sigma}_j , \, (\boldsymbol{\tau}_i \cdot \boldsymbol{\tau}_j)(\boldsymbol{\sigma}_i \cdot \boldsymbol{\sigma}_j) , \, S_{ij} , \, S_{ij}\boldsymbol{\tau}_i \cdot \boldsymbol{\tau}_j , \qquad (25)$$

are the main static operators that appear in the two-nucleon potential and the $f^p$ are functions of the interparticle distance $r_{ij}$ generated by the solution of a set of coupled differential equations containing the bare two-nucleon potential with asymptotically-confined boundary conditions [32]. In order to study how correlations in the nuclear wave functions impact on the calculated matrix elements, we perform a calculation in which we turn off the "one-pion-exchange-like" correlation operators, *i.e.*, $(\boldsymbol{\tau}_i \cdot \boldsymbol{\tau}_j)(\boldsymbol{\sigma}_i \cdot \boldsymbol{\sigma}_j)$ and $S_{ij}\boldsymbol{\tau}_i \cdot \boldsymbol{\tau}_j$. The effects such an artificial change will be discussed in Sec. IV.

In principle, the variational wave function can be further improved via an imaginary time propagation of the Schrödinger equation. This procedure has the effect of eliminating spurious contributions coming from excited states and it is implemented by the GFMC algorithm [32]. However, Quantum Monte Carlo studies of electroweak matrix elements in low-lying nuclear states of $A \leq 10$ nuclei indicate that the GFMC propagation improves the VMC results by $\lesssim 3\%$ [29, 51], an accuracy that goes beyond the scope of the present investigation.

The results presented below for $A \leq 10$ nuclei use the VMC wave functions that serve as starting trial functions for the GFMC calculations summarized in Ref. [32]. We emphasize that the $A = 12$ matrix elements are based on the first quantum Monte Carlo wave function for $^{12}$Be. For the $A = 12$ nuclei, we use new clusterized variational wave functions that provide for alpha- and dineutron-like clusters among the p-shell nucleons. As for the lighter nuclei, they are fully antisymmetric $A$-body wave functions, translationally invariant, and include the same product of two- and three-body operator correlations induced by the nuclear Hamiltonian. However, for simplicity, only the highest spatial symmetry states are used, i.e., [444] in $^{12}$C and [4422] in $^{12}$Be, as specified in Young diagram notation [52]. The construction of $^{12}$C can be thought of as coupling a core $^8$Be nucleus in one of its first three states ($0^+$, $2^+$, or $4^+$) with an additional p-shell alpha-like cluster in respectively a $^1$S$_0$, $^1$D$_2$, or $^1$G$_4$ state, to give a total $J^\pi = 0$. Similarly, for $^{12}$Be, a core $^8$He nucleus in one of its first two states ($0^+$ or $2^+$) is coupled with a $^1$S$_0$ or $^1$D$_2$ p-shell alpha-like cluster. In both cases a small-basis diagonalization is made among these components. These $A = 12$ calculations are computationally

demanding because of the size of the spin-isospin vectors needed to represent the wave function: 4,096 x 132 for $^{12}$C and 4,096 x 275 for $^{12}$Be, where we assume pure $T = 0$ and $T = 2$ states, respectively. We emphasize that this is the first quantum Monte Carlo wave function for $^{12}$Be.

In addition to presenting results on the matrix elements of Eq. (16), we study their associated transition distributions in $r$-space, $C^{\alpha,\beta}(r)$, and $q$-space, $\bar{C}^{\alpha,\beta}(q)$ defined as

$$M^{\alpha,\beta} = \int d\mathbf{r}\, \rho^{\alpha,\beta}(r) \equiv \int dr\, C^{\alpha,\beta}(r) \equiv \int dq\, \bar{C}^{\alpha,\beta}(q) , \qquad (26)$$

where $\rho^{\alpha,\beta}(r)$ is the transition density associated with the transition operator $O^{\alpha,\beta}(r)$.

Finally, following Ref. [53] we represent the delta-functions entering the $V_{GT,MM}$ and $V_{F,NN}$ potentials defined in Eqs. (A5) and (A7) with

$$\delta(m_\pi \mathbf{r}) = \frac{e^{-(r/R_S)^2}}{m_\pi^3 R_S^3 \pi^{3/2}} , \qquad (27)$$

where $R_S$ is a short range cutoff. We tested the sensitivity of the calculated matrix elements with respect to variations of $R_S \in \{0.6 , 1.0\}$ fm. The matrix elements were found to be stable at the few percent level.

We also analyzed the sensitivity of the GT-AA matrix elements to variation in the regulator function $F(r)$ defined as

$$F(r) = 1 - \frac{1}{(r/R_L)^6 e^{[2(r-R_L)/R_L]} + 1} , \qquad (28)$$

for values of $R_L \in \{0.6 , 0.8\}$ fm. We found a variation of $\lesssim 17\%$ in the calculated isospin-changing matrix elements of $A = 8$–12 decays, a somewhat large variation which arises from a delicate cancellation in the associated GT-AA transition densities (see Sec. IV for explanation). A detailed study focused on the cutoff dependence is beyond the scope of this work, and in what follows we report the matrix elements obtained without the regulator function given above. It would indeed be interesting to reanalyze these systems using different nuclear Hamiltonians. This would allow one to assess the sensitivity to short-distance dynamics and to associate a model dependence uncertainty to the calculations. In particular, Quantum Monte Carlo calculations based on chiral two- and three-body potentials are now feasible [53–55], which opens up the possibility of systematically and consistently studying the sensitivity to cutoff variations in both the nuclear Hamiltonian and $0\nu\beta\beta$-decay potentials. Work along these lines is in progress.

## IV. RESULTS

Before proceeding to the discussion of the results, we emphasize that we use the value of the axial coupling
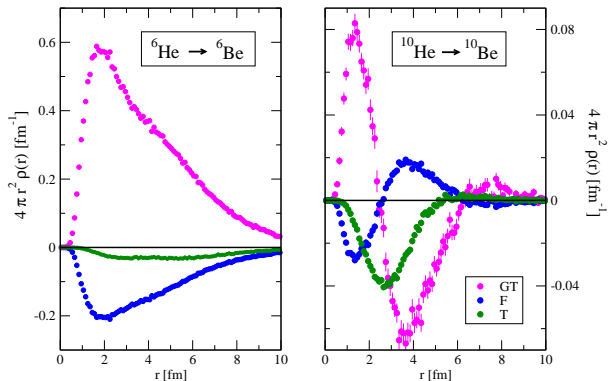
FIG. 2. VMC calculations of the transition densities associated with the F, GT, and T operators—$\sum_{a<b}(\tau_a^+ \tau_b^+)$, $\sum_{a<b}(\boldsymbol{\sigma}_a \cdot \boldsymbol{\sigma}_b\, \tau_a^+ \tau_b^+)$, and $\sum_{a<b}(S_{ab}\, \tau_a^+ \tau_b^+)$, respectively— for the $^6$He→$^6$Be (left panel) and $^{10}$He→$^{10}$Be decays (right panel).

constant $g_A = 1.2723(23)$ [28]. In fact, recent GFMC studies on single-beta decay in $A \leq 10$ nuclei based one the AV18+IL7 model adopted here, indicate that the "$g_A$-problem"—that is the systematic over-prediction of single-beta Gamow-Teller matrix elements in simplified nuclear calculations—can be resolved by correlation effects in the nuclear wave functions [29]. These findings are limited to studies of matrix elements at zero momentum transfer, whereas the average momentum transfer in $0\nu\beta\beta$-decay matrix elements is of the order of $\sim 100$ MeV [25]. It remains to be determined how the "$g_A$-problem" propagates at intermediate values of momentum transfer, and whether the microscopic picture of the nucleus based on the "unquenched" nucleonic weak couplings successfully explains the data in this energy regime. Progress in this direction would be facilitated by the acquisition of neutrino-nucleus scattering data, which are scarce at moderated values of momentum transfer.

In Tables I and II, we list the calculated $0\nu\beta\beta$-decay matrix elements in $^6$He, $^8$He, $^{10}$Be, $^{10}$He, and $^{12}$Be transitions. We identify two classes of transitions, namely transitions in which the total isospin of the initial and final states remains unchanged, i.e., $\Delta T = |T_i - T_f| = 0$, and those in which the total isospin changes by two units, i.e., $\Delta T = 2$. The former involves isobaric analog states, which is never the case in nuclear transitions considered for the actual experiments. It is nevertheless interesting to study these systems with the goal of benchmarking different nuclear models and/or computational methods.

Transition densities between isobaric analog states are characterized by the lack of nodes: this can be appreciated in the left panel of Fig. 2 where we show results for the $^6$He→$^6$Be decay as a representative of this class. Once the VMC nuclear wave function for, e.g. $^6$He, is determined, then that of $^6$Be is obtained from it by swap-

ping protons and neutrons. As a result, the initial and final wave functions differ only in the third component of the isospin, while their radial and spin dependence is the same, implying a maximum overlap between the two wave functions and the consequent lack of nodes in the transition densities. In fact, evaluation of the $\sum_{a<b} \tau_a^+ \tau_b^+$ operator in between these wave functions gives one, i.e., the wave function normalization (this is in case one neglects tiny contributions induced by the isoscalar Coulomb term [56] which is different in the two isobaric analog nuclei due to their different number of protons). Similar considerations apply to the $A = 10$ transitions in this class. The $^8$He and $^8$Be$^\star$ excited state have the same spatial symmetry, predominantly a $^1S_0$-[422], but with different $T_z$ component. In fact, they both have an alpha-like core with $S = T = 0$, whereas the remaining two-nucleon pairs are two $^1S_0$-$(nn)$ dineutrons in $^8$He, and an equal mixture of two $^1S_0$-$(np)$ $T = 1$ pairs, one $^1S_0$-$(nn)$ dineutron and one $^1S_0$-$(pp)$ diproton in $^8$Be. Again, there is no change in the spatial symmetry of the initial and final states.

$\Delta T = 2$ transitions are especially interesting due to their direct correspondence to the experimental cases. As an example of this class, in the right panel of Fig. 2 we show the $^{10}$He→$^{10}$Be transition densities associated with the F, GT, and T operators, namely $\sum_{a<b}(\tau_a^+\tau_b^+)$, $\sum_{a<b}(\boldsymbol{\sigma}_a \cdot \boldsymbol{\sigma}_b\, \tau_a^+\tau_b^+)$, and $\sum_{a<b}(S_{ab}\, \tau_a^+\tau_b^+)$, respectively. Here, the F and GT densities present nodes due to the orthogonality between the dominant spatial symmetries of the initial $[4222]=[\alpha,(nn),(nn),(nn)]$ and final $[442]=[\alpha,\alpha,(nn)]$ wave functions. Note that integrating the F transition density (blue dots labeled with 'F' in the figure) over $d\mathbf{r}$ gives zero, which follows from isospin-conservation. Similarly, nodes are found in the F and GT densities associated with the $A = 8$ and 12 transitions in this class. In particular, the nodes are due to the orthogonality between the dominant spatial symmetries of the initial $[422]=[\alpha,(nn),(nn)]$ ($[4422]=[\alpha,\alpha,(nn),(nn)]$) and final $[44]=[\alpha,\alpha]$ ($[444]=[\alpha,\alpha,\alpha]$) states in the $^8$He→$^8$Be ($^{12}$Be→$^{12}$C) decay. In the remainder of this section we will primarily focus our attention on $\Delta T = 2$ transitions in $A = 10$ and 12, and just report the results obtained for the $A = 8$ decay. In fact, $^8$Be presents a unique and rich structure characterized by a strong two-$\alpha$ cluster in both its ground state—that lies $\sim 0.1$ MeV above the threshold for breakup into two $\alpha$'s—and first two rotational excited states of two $\alpha$ particles rotating about each other [57, 58]. These features make this test case less appealing for comparisons with decays relevant from the experimental point of view.

## A. Light Majorana neutrino exchange

In Table I, we report a breakdown of the tree-level light Majorana-neutrino exchange potentials defined in Eqs. (7)–(9). The first three rows show the results for transitions between isobaric analog states. In this case,
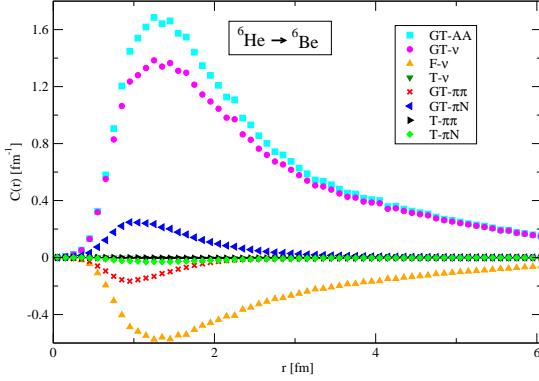
FIG. 3. VMC calculations of the transition distributions $C^{\alpha,\beta}(r)$ defined in Eq. (26) for the $^6\mathrm{He}\to{}^6\mathrm{Be}$ decay.

the absence of nodes implies that the F-$\nu$ and GT-AA contributions dominate the $0\nu\beta\beta$-potentials. The GT-AP and GT-PP components, which have pion-range, steeply fall off for $r \gtrsim 2$ fm, and give, respectively, a $\sim 20\%$ and $\sim 5\%$ correction to the GT-$\nu$ matrix element. This can be appreciated from Fig. 3, which shows that for $r > 2$ fm the total GT distribution $C^{GT,\nu}$ is very well approximated by the AA component. The weak-magnetic term GT-MM, which is a $\mathrm{N}^2\mathrm{LO}$ correction in chiral EFT, is small, about 2%. Fig. 3 also shows that the tensor matrix elements are negligible.

The results for the $\Delta T = 2$ transitions are shown in rows $4-6$ of Table I. The most important feature of these transitions is the presence of nodes, which causes the GT and F densities, illustrated in the right panel of Fig. 2, to change sign at about 2.5 fm. As a result, there is a large cancellation for the F-$\nu$ and GT-AA matrix elements,
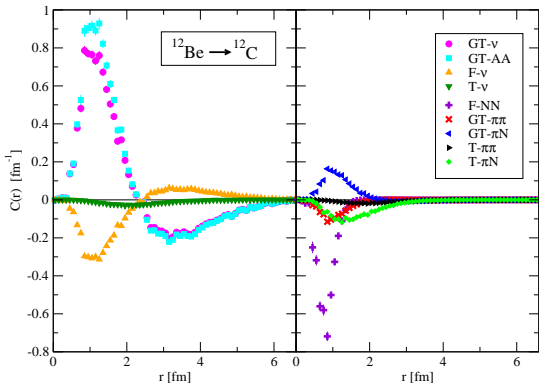


FIG. 4. VMC calculations of the transition distributions $C^{\alpha,\beta}(r)$ defined in Eq. (26) for the $^{12}\mathrm{Be}\to{}^{12}\mathrm{C}$ decay.

which causes these NMEs to be significantly smaller than in the case of transitions involving isobaric analog states. This is illustrated in the left panel of Fig. 4 for the $^{12}\mathrm{Be}\to{}^{12}\mathrm{C}$ transition, where the region with $r > 2.5$ fm reduces the GT-AA matrix element by 50%. The same NMEs were compared in $\Delta T = 2$ and $\Delta T = 0$ transitions of heavier systems, such as $^{48}\mathrm{Ca}\to{}^{48}\mathrm{Ti}$, in Refs. [59, 60], where a similar suppression of the NMEs in $\Delta T = 2$ transitions was found. In contrast, the AP, PP and MM components, which are pion- and short-range contributions, are much less affected by this cancellation, and are therefore more important in the $\Delta T = 2$ transitions. Both of these effects can also be seen from Table I. For example, in the $^{10}\mathrm{He}\to{}^{10}\mathrm{Be}$ transition the AP, PP and MM components are, respectively, 48%, 16% and 10% of the GT-AA, and, while the GT-AA matrix element is 20 times smaller than in the $^6\mathrm{He}\to{}^6\mathrm{Be}$ transition, the AP, PP and MM matrix elements are only about a factor of 5 smaller. Table I also shows a partial cancellation between the GT-AP and GT-PP and GT-MM components, which is a common feature of both $\Delta T = 0$ and $\Delta T = 2$ transitions. As a result we find that the GT-$\nu$ matrix element is always dominated by the GT-AA component. In the case of transitions between isobaric analogues, the GT-AA matrix element is 90% of the total GT-$\nu$ contribution, while in $\Delta T = 2$ transitions, it is approximately 80%. A similar effect is observed in calculations of heavier systems, such as $^{48}\mathrm{Ca}$, $^{76}\mathrm{Ge}$, and $^{136}\mathrm{Xe}$ [30, 31, 61–63]. The T-MM contribution—a contact-like contribution—is statistically zero in both $\Delta T = 0$ and 2. This is a consequence of the fact that the tensor operator $S_{ab}$ vanishes in between $nn$-pairs in relative S-wave, which is the dominant two-nucleon component at short distances.

The absolute size of the NMEs shows sizable variations between different $\Delta T = 2$ transitions. In particular, the matrix elements increase by a factor of 2.5 between the $^{10}\mathrm{He}\to{}^{10}\mathrm{Be}$ and $^{12}\mathrm{Be}\to{}^{12}\mathrm{C}$ transitions. This can be appreciated from Fig. 5, where we show the GT-$\nu$ and F-$\nu$ transition distributions in momentum space. While the shape of the distributions is very similar in the two transitions, the peak is significantly larger in $^{12}\mathrm{Be}\to{}^{12}\mathrm{C}$. This effect may be due, at least partially, to a large difference in the spatial extent of the relevant wave functions. The $^{10}\mathrm{He}$ system is only a resonance, unstable against breakup into $^8\mathrm{He}+2n$ by about 1 MeV. Here we have employed a pseudo-bound (with an exponentially falling density at long range) VMC wave function that is quite diffuse, with a proton (neutron) rms radius of 1.95 (3.66) fm. The $^{10}\mathrm{Be}$, $^{12}\mathrm{Be}$, and $^{12}\mathrm{C}$ nuclei are all bound systems, with VMC wave functions that have proton (neutron) rms radii of 2.32 (2.50) fm, 2.43 (2.99) fm, and 2.48 (2.48) fm, respectively. GFMC calculations change these radii by less than 5%. Thus, for the $A = 10$ decay, two neutrons with an rms radius of 3.66 fm must be converted to two protons at an rms radius of 2.32 fm, indicating a small spatial overlap between the initial and final wave functions and consequently relatively small matrix elements. In comparison, the $A = 12$ decay only requires

TABLE I. VMC calculations of the dimensionless matrix elements, defined in Eq. (16), relevant for light Majorana-neutrino exchange. The first (second) three rows show the results for the $\Delta T = 0$ ($\Delta T = 2$) transitions (see text for explanation). For comparison, the bottom five rows show the results of Refs. [30] and [31] for the heavy nuclei $^{48}$Ca, $^{76}$Ge, and $^{136}$Xe. VMC statistical errors (not reported in the table) are $\lesssim 2\%$.

| $(T_i) \to (T_f)$ | | F | GT | | | | | T | | | | |
|---|---|---|---|---|---|---|---|---|---|---|---|---|
| | | $\nu$ | $AA$ | $AP$ | $PP$ | $MM$ | $\nu$ | $AP$ | $PP$ | $MM$ | $\nu$ | $AA$ |
| $^6$He(1)$\to^6$Be(1) | | -1.502 | 4.114 | -0.692 | 0.164 | 0.103 | 3.688 | -0.032 | 0.010 | -0.004 | -0.025 | -0.099 |
| $^8$He(2)$\to^8$Be$^\star$(2) | | -3.310 | 3.132 | -0.548 | 0.134 | 0.082 | 2.798 | -0.009 | 0.000 | 0.000 | -0.009 | -0.060 |
| $^{10}$Be(1)$\to^{10}$C(1) | | -1.898 | 4.326 | -0.834 | 0.216 | 0.139 | 3.848 | -0.097 | 0.032 | -0.012 | -0.078 | -0.255 |
| $^8$He(2)$\to^8$Be(0) | | -0.097 | 0.152 | -0.117 | 0.042 | 0.030 | 0.108 | -0.026 | 0.010 | -0.004 | -0.021 | -0.058 |
| $^{10}$He(3)$\to^{10}$Be(1) | | -0.078 | 0.196 | -0.094 | 0.032 | 0.020 | 0.156 | -0.032 | 0.012 | -0.004 | -0.026 | -0.074 |
| $^{12}$Be(2)$\to^{12}$C(0) | | -0.192 | 0.500 | -0.240 | 0.084 | 0.056 | 0.400 | -0.066 | 0.024 | -0.010 | -0.052 | -0.142 |
| $^{48}$Ca $\to^{48}$Ti | [30] | -0.25 | 1.08 | -0.38 | 0.13 | 0.10 | 0.93 | -0.08 | 0.03 | -0.01 | -0.06 | – |
| $^{76}$Ge $\to^{76}$Se | [30] | -0.59 | 3.15 | -0.94 | 0.30 | 0.22 | 2.73 | -0.01 | 0.00 | 0.00 | -0.01 | – |
| | [31] | -1.74 | 5.48 | -2.02 | 0.66 | 0.50 | 4.62 | -0.35 | 0.10 | -0.04 | -0.29 | – |
| $^{136}$Xe $\to^{136}$Ba | [30] | -0.54 | 2.45 | -0.79 | 0.25 | 0.19 | 2.10 | 0.01 | -0.01 | 0.00 | 0.00 | – |
| | [31] | -0.89 | 3.17 | -1.19 | 0.39 | 0.31 | 2.67 | -0.28 | 0.09 | -0.03 | -0.22 | – |

a shift from 2.99 fm to 2.48 fm, which leads to a significantly larger spatial overlap, and larger matrix elements. This last transition in $A = 12$ is possibly the test case that is most like $0\nu\beta\beta$ decays in nuclei of experimental interest.

To the best of our knowledge, the first microscopic calculations of transition distributions in $A = 8$ and 10 nuclei have been reported in Ref. [64] within the No-core shell model framework. In that reference, the authors were interested in testing the validity of the Lee-Suzuki mappings and related techniques to construct effective two-body operators, rather than having results based on realistic wave functions. It is nevertheless interesting to compare the two calculations. We find that our NMEs based on VMC wave functions are smaller by a factor of $\sim 40\%$ with respect to those reported in Ref. [64]. We think that this discrepancy is due to the capability of the VMC wave functions of capturing the diffuseness of the $^8$He and $^{10}$He systems. This makes the overlaps with the final $^8$Be and $^{10}$Be smaller with respect to those obtained in the No-core shell model which instead utilize the same oscillator well for both the initial and final states.

As a comparison, in the last five rows of Table I we show the shell model [30, 61, 65] and proton-neutron quasiparticle random-phase approximation [31] for $^{48}$Ca, $^{76}$Ge and $^{136}$Xe. Results form other many-body methods differ by a factor of 2-3 [25]. Although the absolute sizes of these NMEs are larger by a factor of a few than those of the $\Delta T = 2$ transitions calculated here, the relative factors between the different NMEs seem to agree fairly well (see also Table III), indicating that the relative size of long- and short-distant physics is independent of the particular nuclear systems considered.

It is interesting to note that the $R_A$ normalization factor introduced in Eqs. (17)–(19) can induce some misjudgment when comparing results from different nuclei. In fact, if we multiply the NMEs by $1/R_A$ (with $R_8 = 2.40$ fm, $R_{10} = 2.58$ fm, and $R_{12} = 2.75$ fm) we find a remarkably good agreement between short- and pion-range potentials evaluated in $A = 12$ and $A = 48$ with $R_{48} = 4.36$ fm (and, to a lesser extent, $A = 76$ and $A = 136$ with $R_{76} = 5.08$ fm and $R_{136} = 6.17$ fm) decays. This could be due to the fact that short-range operators depend on the nuclear density which is roughly the same in all nuclei.

The last column of Table I reports our results for the matrix element T-AA, which does not contribute in the case of light Majorana-neutrino exchange, but it is relevant in the presence of right-handed charged-currents [22, 44, 45]. This matrix element is not often computed in the literature, and in Ref. [22] bounds on the right-handed operator $C_{\rm VR}^{(6)}$ were obtained setting $M_{T,AA} = 0$. If we naively assume that the ratio between the GT-AA and T-AA matrix elements is the same in heavy and light nuclei, a T-AA matrix element of the size reported in Table I would affect the bounds on $C_{\rm VR}^{(6)}$ at the 20% level.

The results discussed in this section, summarized in Table I, deal mostly with NMEs involved in light Majorana-neutrino exchange. However, as noted in Ref. [22], linear combinations of the same NMEs determine additional long-range contributions to $0\nu\beta\beta$ mediated by dimension-six and -seven LNV semileptonic operators, that are not proportional to $m_{\beta\beta}$.

## B. LNV from short-distance

We now discuss the neutrino potentials induced by dimension-nine operators, which do not involve neutrino exchange, but are pion- or short-range. Our results are summarized in Table II, where the first and middle three rows give the $\Delta T = 0$ and $\Delta T = 2$ transitions, respectively. For comparison, the bottom three rows give the results of Ref. [30] for the corresponding NMEs in heavier systems.

By power counting, with the definitions in Eqs. (7)–(9)

TABLE II. VMC results for the dimensionless matrix elements, defined in Eq. (16), relevant for the contributions of the dimension-nine operators in Eq. (2). For comparison, we also show the total matrix elements for the light Majorana neutrino mechanism. The first (second) three rows show the results for the $\Delta T = 0$ ($\Delta T = 2$) transitions (see text for explanation). For comparison, the bottom three rows show the results of [30] for the heavy nuclei $^{48}$Ca, $^{76}$Ge, and $^{136}$Xe. VMC statistical errors (not reported in the table) are $\lesssim 2\%$.

| $(T_i) \rightarrow (T_f)$ | F | | GT | | | | T | | |
|---|---|---|---|---|---|---|---|---|---|
| | $\nu$ | $NN$ | $\nu$ | $\pi\pi$ | $\pi N$ | $NN$ | $\nu$ | $\pi\pi$ | $\pi N$ |
| $^{6}$He(1)$\rightarrow^{6}$Be(1) | -1.502 | -0.586 | 3.688 | -0.160 | 0.354 | 1.740 | -0.025 | -0.009 | -0.040 |
| $^{8}$He(2)$\rightarrow^{8}$Be$^{\star}$(2) | -3.310 | -0.532 | 2.798 | -0.128 | 0.276 | 1.414 | -0.009 | 0.000 | 0.015 |
| $^{10}$Be(1)$\rightarrow^{10}$C(1) | -1.898 | -0.876 | 3.848 | -0.218 | 0.432 | 2.588 | -0.078 | -0.032 | -0.148 |
| $^{8}$He(2)$\rightarrow^{8}$Be(0) | -0.097 | -0.198 | 0.108 | -0.044 | 0.058 | 0.596 | -0.021 | -0.010 | -0.053 |
| $^{10}$He(3)$\rightarrow^{10}$Be(1) | -0.078 | -0.134 | 0.156 | -0.032 | 0.046 | 0.402 | -0.026 | -0.012 | -0.057 |
| $^{12}$Be(2)$\rightarrow^{12}$C(0) | -0.192 | -0.370 | 0.400 | -0.084 | 0.120 | 1.106 | -0.052 | -0.022 | -0.122 |
| $^{48}$Ca $\rightarrow^{48}$Ti | -0.25 | -0.64 | 0.93 | -0.12 | 0.18 | 2.11 | -0.060 | -0.026 | -0.153 |
| $^{76}$Ge $\rightarrow^{76}$Se | -0.59 | -1.46 | 2.73 | -0.31 | 0.49 | 4.87 | -0.010 | 0.00 | -0.026 |
| $^{136}$Xe $\rightarrow^{136}$Ba | -0.54 | -1.28 | 2.1 | -0.26 | 0.42 | 4.25 | -0.010 | 0.00 | 0.026 |

TABLE III. The Table shows the same matrix elements as Table II, relevant for dimension-nine contributions, now normalized to the GT-$AA$ (GT-$\pi N$) matrix element in the left (right) panel. For comparison, the results of [30, 31] for $^{48}$Ca, $^{76}$Ge and $^{136}$Xe are shown.

| $(T_i) \rightarrow (T_f)$ | | F | | GT | | | | F | GT | |
|---|---|---|---|---|---|---|---|---|---|---|
| | | $\nu$ | $NN$ | $AA$ | $\nu$ | $\pi\pi$ | $\pi N$ | $NN$ | $\pi\pi$ | $\pi N$ |
| $^{8}$He(2)$\rightarrow^{8}$Be(0) | | -0.63 | -1.37 | 1 | 0.71 | -0.28 | 0.38 | 3.38 | -0.76 | 1 |
| $^{10}$He(3)$\rightarrow^{10}$Be(1) | | -0.39 | -0.71 | 1 | 0.79 | -0.16 | 0.23 | 2.86 | -0.68 | 1 |
| $^{12}$Be(2)$\rightarrow^{12}$C(0) | | -0.38 | -0.77 | 1 | 0.80 | -0.17 | 0.24 | 3.08 | -0.70 | 1 |
| $^{48}$Ca $\rightarrow^{48}$Ti | [30] | -0.23 | -0.60 | 1 | 0.86 | -0.11 | 0.17 | 3.55 | -0.68 | 1 |
| $^{76}$Ge $\rightarrow^{76}$Se | [30] | -0.19 | -0.46 | 1 | 0.87 | -0.10 | 0.15 | 2.97 | -0.63 | 1 |
| | [31] | -0.32 | -0.63 | 1 | 0.84 | -0.12 | 0.19 | 3.34 | -0.66 | 1 |
| $^{136}$Xe $\rightarrow^{136}$Ba | [30] | -0.22 | -0.52 | 1 | 0.86 | -0.10 | 0.17 | 3.06 | -0.59 | 1 |
| | [31] | -0.28 | -0.48 | 1 | 0.84 | -0.11 | 0.16 | 3.03 | -0.68 | 1 |

and (12), one would expect all the NMEs in Table II to be of similar size. In the case of the $\Delta T = 0$ transitions, however, the lack of nodes is responsible for the dominance of the GT-$\nu$ and F-$\nu$ NMEs over the other matrix elements listed in Table II. The GT-$\pi\pi$ and GT-$\pi N$ contributions are, respectively, only $\sim 5\%$ and $\sim 10\%$ of the GT-$\nu$ matrix element. As these NMEs are proportional to GT-PP and GT-AP matrix elements, this is what we would expect from the results in Table I. In Figs. 3 and 4 we can see how the transition distributions associated with the pion-exchange operators $\pi\pi$ and $\pi N$ start to die off at $\sim 1$ fm, which is expected since the range of these operators is approximately set by $1/m_\pi \sim 1.4$ fm. We also note that T-like operators are highly suppressed, as can be seen from the figures as well as from Table II. As discussed in the previous session, this is a consequence of the fact that the tensor operator $S_{ab}$ vanishes in between $nn$-pairs in relative S-wave, which is the dominant two-nucleon component at short distances.

For the $\Delta T = 2$ class, we show in Fig. 4 the calculated distributions of the $^{12}$Be$\rightarrow^{12}$C transition. Due to the characteristic node in the GT transition densities and the ensuing cancellation, the GT-$\pi\pi$ (GT-$\pi N$) matrix element of this class is found to be as large as $\sim 30\%$

($\sim 40\%$) of the GT-$\nu$ contribution (see Table II). This is (numerically) consistent with the results for the GT-PP and GT-AP matrix elements of Table I. One can again see that the GT-$\pi\pi$ and GT-$\pi N$ distributions start to fall off around 1.1 fm, and that the T-like operators are highly suppressed for the $\Delta T = 2$ transitions as well. From comparing the last six rows of Table II one can see that the absolute sizes of the matrix elements calculated here are smaller by a factor of a few than those calculated for heavier systems. In Table III we show the F and GT matrix elements normalized to the GT-AA and GT-$\pi N$ components, including, for heavy system, results obtained with two many-body methods, the shell-model [30] and the quasiparticle random phase approximation [31]. From the left panel we see that, in a given method, the relative importance of long-, pion- and short-range potentials is fairly constant, and the hierarchy of matrix elements is the same for heavy and light nuclei. For pion- and short-distance matrix elements, we observe an even better agreement. As illustrated in the right panel, after normalizing to GT-$\pi N$, the normalized short-range matrix elements of light and heavy nuclei, and of heavy nuclei computed with different methods, are consistent at the 20% level or better.
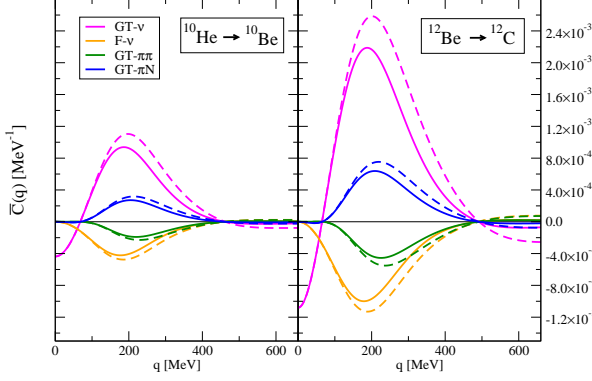
FIG. 5. The GT-$\nu$, F-$\nu$, GT-$\pi\pi$, and GT-$\pi N$ distributions in momentum space for the $^{10}$He$\rightarrow^{10}$Be and $^{12}$Be$\rightarrow^{12}$C decays. Solid and dashed lines are obtained, respectively, with and without the inclusion of the momentum dependence in nucleonic form factors. See text for explanation.



FIG. 6. The left (right) panel shows the GT-AA distribution in $r$-space ($q$-space) for the $^{10}$He$\rightarrow^{10}$Be transition, with and without "one-pion-exchange-like" correlations in the nuclear wave functions. See text for explanation.

Finally, to obtain the short-range matrix elements GT-NN and F-NN we used the regularization of the delta function potential in Eq. (27). If we instead regulate the divergence by using a dipole form factor, either $g_V(\mathbf{q}^2)$ or $g_A(\mathbf{q}^2)$, the NMEs vary by no more than a few percent. The relation GT-NN$= -3$ F-NN is very accurately satisfied by the matrix elements in Tab. II.

## C. Sensitivity to form factors and correlations

We now turn our attention to the sensitivity of the matrix elements to variations in the nucleonic form factors as well as variations in the nuclear wave functions' correlations. To this end we study in more detail the $\Delta T = 2$ transition $^{10}$He$\rightarrow^{10}$Be and report our results in Table IV. The findings discussed in this section in relation to the $A = 10$ decay apply to the other $\Delta T = 2$ transitions considered in the present work as well.

The neutrino potentials in Eqs. (7)–(9) include the vector and axial form factors $g_V(\mathbf{q}^2)$ and $g_A(\mathbf{q}^2)$, whose momentum dependence is an N$^2$LO correction in chiral EFT. To study the impact of these form factors, we repeated the calculation of the NMEs setting $g_V(\mathbf{q}^2) = 1$ and $g_A(\mathbf{q}^2) = g_A$. We report the results for the $^{10}$He$\rightarrow^{10}$Be transition in the second row of Table IV. For the F-$\nu$ and GT-$\nu$ matrix elements the effect of turning off the axial and vector form factors is mild, resulting in at most a 10% increase. For the T-AP and the T-PP components, this effect appears to be larger, $\sim 20\%$-30%. In $\Delta T = 2$ transitions the variation is magnified by the cancellations that affect the F and GT-AA matrix elements. For comparison, in $\Delta T = 0$ transitions the effect of turning off the momentum dependence of $g_{V,A}(\mathbf{q}^2)$ is less than 5%.
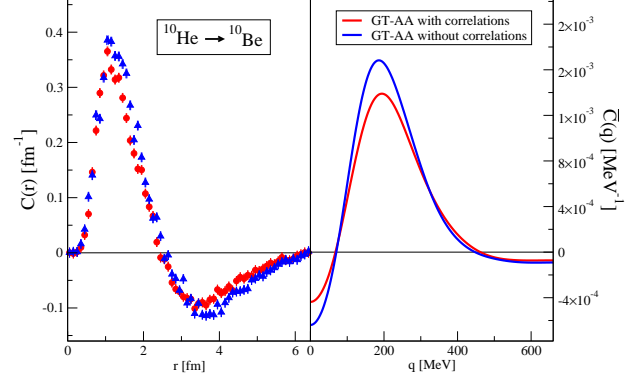
For the weak-magnetic contributions GT-MM, some care has to be taken when removing the form factors. As evident from Eqs. (A5) and (A6), in the absence of $g_V(\mathbf{q}^2)$, both $V_{GT,MM}$ and $V_{T,MM}$ are singular at $r \rightarrow 0$. To compute the GT-MM matrix element in the second line of Table IV we used the regularization of the delta function in Eq. (27), with $R = 0.6$ fm. Varying $R$ between 0.6 and 0.8 fm does not have an appreciable effect on the result. The good agreement for the values of GT-MM in the first and second line of Table IV indicates that the result does not strongly depend on the way the region of large $\mathbf{q}^2$ is regulated. For the T-MM matrix element, the second line of Table IV is obtained by naively using the potential $V_{T,MM}(r)$ in Eq. (A6). Here the divergence at $r = 0$ does not spoil the evaluation of the associated matrix element. Again this is due to the fact that the tensor operator T $(S_{ab})$ gives zero on pairs in relative S-wave. In fact, the $\tau_a^+\tau_b^+$ is selecting out valence $(nn)$ pairs in the initial state. These are largely in a $^1S_0$ relative state, with some $^3P_0$ components which are however zero at short-range due to an angular momentum barrier.

While in Table IV we only report results for the impact of form factors on the light neutrino-exchange potentials, the same features are shared by matrix elements of the $V_{\pi\pi}$ and $V_{\pi N}$ potentials, as they are proportional to to the AP and PP components in IV. The same holds for the $V_{NN}$ potential, which is analogous to GT-MM. In particular, changing the regularization of the delta function potential from Eq. (27) to a dipole form factor, either $g_V(\mathbf{q}^2)$ or $g_A(\mathbf{q}^2)$ has little effect on the F-NN and GT-NN matrix elements.

The impact of the axial and vector form factors on the $^{10}$He$\rightarrow^{10}$Be and $^{12}$Be$\rightarrow^{10}$C transitions is illustrated in Fig. 5. The solid and dashed lines denote the distributions $\bar{C}(q)$ defined in Eq. (26), with and without the dipole form factors for $g_{V,A}(\mathbf{q}^2)$. We see that the dipole

form factors start to have an effect at around $q \sim 200$ MeV, and cut off the distributions for $q \gtrsim 500$ MeV. The effect is similar for the F-$\nu$ and GT-$\nu$, which are mostly long-distance, and the pion-range GT-$\pi\pi$ and GT-$\pi N$ matrix elements, which are induced by heavy LNV new physics.

In the third row of Table IV, we report results obtained by regulating the matrix elements with the $F(r)$ function defined in Eq. (28) with $R_L = 0.7$ fm. We studied the sensitivity of our results with respect to variation of $R_L \in \{0.6, 0.8\}$ fm and found that the most affected matrix elements are those characterized by the presence of the node. For example, by comparing the second and the third rows in the table we can see that GT-$\nu$ and F-$\nu$ undergo a $\sim 18\%$ and $\sim 13\%$ variation, respectively, whereas T-$\nu$ is essentially unaffected by the regulator function. This is because the T-like operators are already zero at short-distances.

Finally, in the forth row of Table IV we report results obtained by artificially turning off the "one-pion-exchange-like" correlation operators in the nuclear wave functions as discussed in Sec. III. Turning the correlations off has a dramatic effect on the tensor matrix elements, which become statistically equal to zero. The GT-$\nu$ and F-$\nu$ magnitudes increase by $\sim 10\%$ with respect to the correlated results given in the first row of the table. The effect of the "one-pion-exchange-like" correlations is represented in Fig. 6, where the blue triangles (solid line) in the left (right) panel represent the $r$-space ($q$-space) GT-AA transition distribution obtained by turning off the correlations to be compared with the red dots (solid line) obtained with the correlated wave function.

In closing this section, we reiterate that $0\nu\beta\beta$ matrix elements involve on average values of momentum transfer $q$ of the order of hundreds of MeVs. This can be seen, for example, in Fig. 5 where the momentum distributions [1] in both the $A = 10$ and 12 decays peak at $\sim 200$ MeV.

### D. Light neutrino exchange beyond leading order

Beyond leading order, several new contributions to light Majorana-neutrino exchange arise. At N²LO in the Weinberg counting, these consist of corrections to the single-nucleon currents as well as contributions to a genuine two-body potential that cannot be absorbed by the one-body weak currents [46]. In addition, at N³LO there are two-body effects in the weak currents (see Refs. [41–43]), which lead to three-nucleon potentials that we will not consider further here. Instead, the N²LO two-body

potentials are induced by loop diagrams involving the neutrino, as well as counterterms that appear at the same order. The corrections to the one-body currents are often included in the $0\nu\beta\beta$ literature through the form factors in Eq. (10), while the two-body contributions have so far not been implemented in nuclear calculations. Here we investigate the impact of this second type of corrections, which appears at the same order as the effect of the form factors discussed in Section IV C.

The N²LO correction to the neutrino-exchange potential of Eq. (6) was derived in Ref. [46] and can be written as

$$V_{\nu,2} = \tau_a^+ \tau_b^+ \left( V_{VV}^{(a,b)} + V_{AA}^{(a,b)} + V_{CT}^{(a,b)} + V_{\mathrm{us}}^{(a,b)} \ln \frac{m_\pi^2}{\mu_{\mathrm{us}}^2} \right),$$
(29)

where $V_{VV}^{(a,b)}$ ($V_{AA}^{(a,b)}$) arises from loops with two insertions of the vector (axial) current, $V_{\mathrm{us}}$ is generated by loops involving ultrasoft neutrinos, and $V_{CT}^{(a,b)}$ captures the counterterm contributions. The latter term involves three counterterms which absorb the renormalization scale ($\mu$) dependence of divergent loop diagrams. We write these pieces as follows [2],

$$\begin{aligned} V_{CT}^{(a,b)} = &\left( \frac{5}{6} g_\nu^{\pi\pi} + 3 L_\pi \right) V_{CT,\pi\pi}^{(a,b)} \\ &+ \left( g_\nu^{\pi N} + (1 - g_A^2) L_\pi \right) V_{CT,\pi N}^{(a,b)} \\ &+ \left( g_\nu^{NN} + \frac{3}{8}(1 - g_A^2)^2 L_\pi \right) V_{CT,NN}^{(a,b)} , \end{aligned}$$
(30)

where $L_\pi = \ln \frac{\mu^2}{m_\pi^2}$ and $g_\nu^{\pi\pi}, g_\nu^{\pi N}$, and $g_\nu^{NN}$ are the counterterms.

It should be noted that the potential in Eq. (29) does not capture the complete N²LO correction. Firstly, the loops involving ultrasoft neutrinos (captured by $V_{\mathrm{us}}$) are divergent and induce the dependence on the renormalization scale $\mu_{\mathrm{us}}$ in Eq. (29). This $\mu_{\mathrm{us}}$ dependence is canceled by ultrasoft contributions to the $0\nu\beta\beta$ amplitude. However, the calculation of these contributions requires knowledge of the intermediate states [46] and is beyond the scope of the current work. Secondly, although $g_\nu^{\pi\pi}$ can be estimated through a connection to electromagnetic corrections to $\pi\pi$ interactions [67], leading to [46] $g_\nu^{\pi\pi}(\mu = m_\rho) = -7.6$, the counterterms $g_\nu^{\pi N}$ and $g_\nu^{NN}$ are currently unknown. Without these missing pieces we do not have full control over the complete N²LO correction. Nevertheless, a rough estimate of the size of the counterterm and the ultrasoft contributions can be obtained by varying the renormalization scales, $\mu$ and $\mu_{\mathrm{us}}$, respectively, such that the logarithms change

---

[1] We point out that with our definition of GT-AA potential given in Eq. (11), the associated $q$-space transition distribution does not go to zero at $q = 0$ (see Figs. 5 and 6). The different behavior at $q = 0$ that is found in the literature [66] is due to the different definition of GT-AA potential, which in the latter case includes the so-called closure energy [25].

[2] With these definitions, $V_{VV,AA}$ and $V_{\mathrm{us}}$ correspond to $\mathcal{V}_{VV,AA}$ and $\tilde{\mathcal{V}}_{AA}$ of Ref. [46] with $L_\pi = 0$, while $V_{CT}$ includes $\mathcal{V}_{CT}$ as well as the $L_\pi$ pieces of $\mathcal{V}_{VV,AA}$. We neglected the contribution of the contact interaction, $C_T$, everywhere.

TABLE IV. VMC calculations of the dimensionless matrix elements relevant for light Majorana-neutrino exchange, defined in Eqs. (A2)–(A4), for the $^{10}$He→$^{10}$Be transition. The first row repeats the results of Table I, which include both the form factors and correlations. The results reported in the second row neglect the momentum dependence in the axial, vector and pseudoscalar nucleonic form factors. Results in the third row are obtained including the regulator given in Eq. (28). Results in the forth row are obtained turning off the "one-pion-exchange-like" correlations in the nuclear wave functions (see text for explanation). VMC statistical errors (not reported in the table) are $\lesssim 2\%$.

| $(T_i) \to (T_f)$ | F | GT | | | | | T | | | |
|---|---|---|---|---|---|---|---|---|---|---|
| | $\nu$ | $AA$ | $AP$ | $PP$ | $MM$ | $\nu$ | $AP$ | $PP$ | $MM$ | $\nu$ |
| $^{10}$He(3)→$^{10}$Be(1) | -0.078 | 0.196 | -0.094 | 0.032 | 0.020 | 0.156 | -0.032 | 0.012 | -0.004 | -0.026 |
| no form factors | -0.088 | 0.218 | -0.098 | 0.034 | 0.020 | 0.172 | -0.042 | 0.016 | -0.006 | -0.032 |
| $F(r)$, $R_L = 0.7$ fm | -0.076 | 0.180 | -0.086 | 0.028 | 0.013 | 0.141 | -0.041 | 0.015 | -0.006 | -0.033 |
| no correlations | -0.086 | 0.222 | -0.106 | 0.036 | 0.022 | 0.172 | -0.004 | 0.002 | 0.000 | -0.004 |

by O(1) (this corresponds to Naive Dimensional Analysis (NDA)).

With the above caveats in mind, we find in the case of the $^{10}$He→$^{10}$Be transition

$$\frac{M_{VV}}{M_\nu} = 7.1 \cdot 10^{-3}, \quad \frac{M_{AA}}{M_\nu} = -7.9 \cdot 10^{-2},$$

$$\frac{M_{CT,\pi\pi}}{M_\nu} = 8.5 \cdot 10^{-3}, \quad \frac{M_{CT,\pi N}}{M_\nu} = -3.8 \cdot 10^{-3},$$

$$\frac{M_{CT,NN}}{M_\nu} = 1.4 \cdot 10^{-2}, \quad \frac{M_{us}}{M_\nu} = -2.4 \cdot 10^{-2}, \quad (31)$$

where $M_\nu$ denotes the matrix element of the potential in Eq. (7), $M_\nu = -M_{F,\nu} + g_A^2(M_{GT,\nu} + M_{T,\nu})$ which can be read from Table I. For the $^{10}$He→$^{10}$Be transition, one has $M_\nu \simeq 0.29$. It should be noted that the potential in Eq. (29) has a divergence for $q \to \infty$ (or $r \to 0$), making it rather sensitive to the way short-distance scales are regulated. Here we naively regulated this divergence by multiplying all terms by $g_A^2(\mathbf{q}^2)/g_A^2$.

The sizes of the different pieces in Eq. (31) vary from the sub-percent level to O(10%) of the LO matrix element, $M_\nu$, which is consistent with the expected size of N$^2$LO corrections. As a result, some of the larger terms in Eq. (31) are of the same order of magnitude as the effects of including the form factors. NDA estimates of the counterterms do not alter this conclusion. However, one should note that the NDA scaling of $g_\nu^{NN}$ is far from obvious in the context of chiral EFT. As discussed in Ref. [46], further work to determine the scaling of $g_\nu^{NN}$ and its possible enhancement is needed.

## V. CONCLUSION

The nuclear *ab initio* approach aims at describing the widest range of nuclear properties in terms of interactions occurring between nucleons inside the nucleus. In this microscopic picture, nucleons interact with each other via two- and three-body interactions, and with external electroweak probes via couplings to individual nucleons and to nucleon-pairs. *Albeit* limited to light nuclei ($A \leq 12$), Quantum Monte Carlo calculations based on the AV18 two-body and IL7 three-body interactions successfully explain available experimental data in a broad energy range, from the keV regime relevant to astrophysics studies to the GeV regime where short-range correlations become predominant [32–34]. These studies yield a rather complex picture of the nucleus with many-body correlations in both the nuclear wave functions and electroweak currents playing an important role in reaching agreement with the data.

In this work, we used the *ab initio* approach supported by the computationally accurate Quantum Monte Carlo methods to study $0\nu\beta\beta$ matrix elements in $A = 6$–$12$ nuclei. While these systems are not relevant from the experimental point of view, they are nevertheless interesting and provide us with an extremely useful set of test cases. In fact, the $0\nu\beta\beta$ rate depends on matrix elements that are not experimentally accessible and need to be estimated theoretically. At present, the calculated nuclear matrix elements of experimental interest ($A \geq 48$) have large theoretical uncertainties which complicate the interpretation of any future $0\nu\beta\beta$ observation or lack thereof. The uncertainties on the calculated matrix elements are primarily attributable to the fact that for larger nuclear systems, in order for the calculations to be computationally feasible, one has to (drastically) approximate the *ab initio* framework, by, *e.g.*, leaving out correlations and/or truncate the model space.

It is in this context that this study on $0\nu\beta\beta$ in light nuclei finds its relevance. For a start, we provided a set of VMC calculations that can be used for benchmarking purposes. We have presented results for the nuclear matrix elements relevant for the light Majorana-neutrino exchange mechanism (Table I) as well as for TeV-scale mechanisms of lepton-number violation (Table II), and we have studied their relative size (see Table III).

Our results for the $\Delta T = 2$ transitions show the following features: (i) The matrix elements for $A = 10, 12$ are between an order of magnitude and a factor of two smaller compared to shell model results for systems with $A = 48, 76, 136$. The bulk of this difference can be attributed to the normalization factor $R_A$ entering Eqs. (17)–(19). (ii) The difference in the $A = 10$ and $A = 12$ matrix elements is correlated with the height of the peaks in their associated transition densities (see Fig. 5) and it is due to the different spatial overlaps be-

tween an initial diffuse neutron distribution and a final compact proton distribution in the case of the $A = 10$ transition, and between two compact initial neutron and final proton distributions in the $A = 12$ transition. (iii) As illustrated in Table III, the ratios of different matrix elements to the dominant Gamow-Teller one (GT-AA) are, in a given method, roughly independent of $A$. We find that for $A = 10, 12$, the ratios agree at the 5% level, while for $A = 48, 76, 136$ they agree at the 15% level or better, and are consistent with the $A = 10, 12$ results at the 30% level. However, if we normalize the GT-like matrix elements by a short-range contribution, *e.g.*, GT-$\pi N$, then the normalized short-range matrix elements are consistent at the $\sim 20\%$ level or better in all the considered nuclear transitions.

Our results will help the community assess the adequacy of the various methods used to estimate $0\nu\beta\beta$ matrix elements, and identify the key dynamical features that need to be retained in more approximate many-body computational methods. This is especially relevant for benchmarking those methods that can be extended to the heavier systems of experimental interest. In this spirit, we have studied the effect of artificially turning off correlations in the VMC nuclear wave functions, finding a $\sim 10\%$ increase in the calculated nuclear matrix elements for the light Majorana neutrino exchange mechanism. This corresponds to having to "quench" $g_A$ by $\sim 0.95$ to accommodate for correlation effects. On the other hand, shell model calculations of single-beta decays [68] indicate that the required "quenching" of $g_A$ in, *e.g.*, the $^{10}$C weak transition, is $\sim 0.83$. These findings may indicate that the $g_A$ "quenching" required in calculations based on more approximated nuclear models (for $A > 12$ nuclei) is larger in single beta decay than in neutrinoless double beta decays.

Within the VMC approach, we have also explored the impact of using different forms for the transition operators mediating $0\nu\beta\beta$ – another potential source of uncertainty in the matrix elements of physical interest. In particular, for the light Majorana-neutrino exchange mechanism, following the chiral EFT approach of Ref. [46] we have estimated the impact of N²LO corrections (in the Weinberg power counting) on the $^{10}$He→$^{10}$Be transition. The "factorizable" N²LO effects captured by nucleon form factors impact the matrix elements at the 10% level (see Table IV). The non-factorizable genuinely two-body effects are discussed in Section IV D. While we do not have full control over the N²LO amplitude (counterterms and ultrasoft contributions are not yet known), our results suggest that the non-factorizable effects may lead to O(10%) corrections, consistently with the expectations of the chiral power counting. Counterterms of the size implied by naive dimensional analysis would not change this conclusion. One should keep in mind, however, that the NDA scaling of the four-nucleon coupling $g_\nu^{NN}$ cannot be taken for granted [46], and further work to check the consistency of Weinberg power counting for $0\nu\beta\beta$ and to determine the scaling of $g_\nu^{NN}$

is needed. In a similar vein, future work should focus on a more consistent chiral EFT approach, in which the nuclear wave functions are determined from a chiral potential. In addition, it would be interesting to examine the three-body potentials induced by chiral EFT two-body axial currents [69, 70]. Work along these lines is in progress.

## Appendix A: Neutrino potentials in coordinate space

Neglecting the momentum dependence of the axial and vector form factors, the potentials in coordinate space read

$$
\begin{aligned}
V_\nu &= m_\pi \tau_a^+ \tau_b^+ \Big( \mathbf{1} \times \mathbf{1}\, V_F^\nu(z) \\
&\quad - g_A^2\, \boldsymbol{\sigma}_a \cdot \boldsymbol{\sigma}_b\, V_{GT}^\nu(z) \;-\; g_A^2\, S_{ab}\, V_T^\nu(z) \Big)\,, \\
V_{\pi\pi} &= -m_\pi \tau_a^+ \tau_b^+\, (\boldsymbol{\sigma}_a \cdot \boldsymbol{\sigma}_b\, V_{GT,\pi\pi}(z) \;+\; S_{ab}\, V_{T,\pi\pi}(z))\,, \\
V_{\pi N} &= -m_\pi \tau_a^+ \tau_b^+\, (\boldsymbol{\sigma}_a \cdot \boldsymbol{\sigma}_b\, V_{GT,\pi N}(z) \;+\; S_{ab}\, V_{T,\pi N}(z))\,, \\
V_{NN} &= m_\pi \tau_a^+ \tau_b^+\, V_{F,NN}(z)\,,
\end{aligned}
\tag{A1}
$$

where $S_{ab}(\hat{r}) \equiv 3\,\boldsymbol{\sigma}_a \cdot \hat{\mathbf{r}}\,\boldsymbol{\sigma}_b \cdot \hat{\mathbf{r}} - \boldsymbol{\sigma}_a \cdot \boldsymbol{\sigma}_b$, and we have introduced $z = r m_\pi$, with $r$ indicating the distance between particles $a$ and $b$. The light Majorana neutrino exchange potentials $V_F^\nu$, $V_{GT}^\nu$ and $V_T^\nu$ are

$$
V_{F,\nu}(z) = \frac{1}{4\pi z},
\tag{A2}
$$

$$
\begin{aligned}
V_{GT,\nu}(z) &= V_{GT,AA}(z) + V_{GT,AP}(z) \\
&\quad + V_{GT,PP}(z) + V_{GT,MM}(z)\,,
\end{aligned}
\tag{A3}
$$

$$
V_{T,\nu}(z) = V_{T,AP}(z) + V_{T,PP}(z) + V_{T,MM}(z)\,,
\tag{A4}
$$

where the GT functions are given by

$$V_{GT,AA}(z) = \frac{1}{4\pi z} \ , \quad V_{GT,AP}(z) = -\frac{e^{-z}}{6\pi z} \ ,$$

$$V_{GT,PP}(z) = -\frac{e^{-z}(z-2)}{24\pi z} \ ,$$

$$V_{GT,MM}(z) = \frac{(1+\kappa_1)^2 \, m_\pi^2}{6g_A^2 m_N^2} \delta^{(3)}(m_\pi \mathbf{r}) \ . \quad \text{(A5)}$$

The tensor functions are

$$V_{T,AP}(z) = \frac{1}{4\pi z^3}\left(2 - \frac{2}{3}e^{-z}(3 + 3z + z^2)\right) \ ,$$

$$V_{T,PP}(z) = -\frac{e^{-z}(1+z)}{24\pi z} \ ,$$

$$V_{T,MM}(z) = \frac{(1+\kappa_1)^2 \, m_\pi^2}{12g_A^2 m_N^2}\frac{3}{4\pi z^3} \ . \quad \text{(A6)}$$

The pion- and short-range potentials induced by dimension-nine $\Delta L = 2$ operators are

$$V_{GT,\pi\pi}(z) = -V_{GT,PP} \qquad V_{T,\pi\pi}(z) = -V_{T,PP}$$

$$V_{GT,\pi N}(z) = -\frac{1}{2}V_{GT,AP} \qquad V_{T,\pi N}(z) = \frac{e^{-z}(3+3z+z^2)}{12\pi z^3},$$

$$V_{F,NN} = V_{GT,NN} = \delta^{(3)}(m_\pi \mathbf{r}). \quad \text{(A7)}$$

[1] J. Schechter and J. W. F. Valle, Phys. Rev. **D25**, 2951 (1982).

[2] S. Davidson, E. Nardi, and Y. Nir, Phys. Rept. **466**, 105 (2008), arXiv:0802.2962 [hep-ph].

[3] J. Argyriades *et al.* (NEMO), Phys. Rev. **C80**, 032501 (2009), arXiv:0810.0248 [hep-ex].

[4] J. Argyriades *et al.* (NEMO-3), Nucl. Phys. **A847**, 168 (2010), arXiv:0906.2694 [nucl-ex].

[5] N. Ackerman *et al.* (EXO-200), Phys. Rev. Lett. **107**, 212501 (2011), arXiv:1108.4193 [nucl-ex].

[6] M. Agostini *et al.* (GERDA), J. Phys. **G40**, 035110 (2013), arXiv:1212.3210 [nucl-ex].

[7] A. Gando *et al.* (KamLAND-Zen), Phys. Rev. **C85**, 045504 (2012), arXiv:1201.4664 [hep-ex].

[8] C. Alduino *et al.* (CUORE), Eur. Phys. J. **C77**, 13 (2017), arXiv:1609.01666 [nucl-ex].

[9] R. Saakyan, Ann. Rev. Nucl. Part. Sci. **63**, 503 (2013).

[10] A. Gando *et al.* (KamLAND-Zen), Phys. Rev. Lett. **117**, 082503 (2016), [Addendum: Phys. Rev. Lett.117,no.10,109903(2016)], arXiv:1605.02889 [hep-ex].

[11] K. Alfonso *et al.* (CUORE), Phys. Rev. Lett. **115**, 102502 (2015), arXiv:1504.02454 [nucl-ex].

[12] J. B. Albert *et al.* (EXO-200), Nature **510**, 229 (2014), arXiv:1402.6956 [nucl-ex].

[13] M. Agostini *et al.* (GERDA), Phys. Rev. Lett. **111**, 122503 (2013), arXiv:1307.4720 [nucl-ex].

[14] A. Gando *et al.* (KamLAND-Zen), Phys. Rev. Lett. **110**, 062502 (2013), arXiv:1211.3863 [hep-ex].

[15] S. R. Elliott *et al.* (2016) arXiv:1610.01210 [nucl-ex].

[16] S. Andringa *et al.* (SNO+), Adv. High Energy Phys. **2016**, 6194250 (2016), arXiv:1508.05759 [physics.ins-det].

[17] M. Agostini *et al.*, Nature **544**, 47 (2017), arXiv:1703.00570 [nucl-ex].

[18] S. Weinberg, Phys. Rev. Lett. **43**, 1566 (1979).

[19] K. S. Babu and C. N. Leung, Nucl. Phys. **B619**, 667 (2001), arXiv:hep-ph/0106054 [hep-ph].

[20] A. de Gouvea and J. Jenkins, Phys. Rev. **D77**, 013008 (2008), arXiv:0708.1344 [hep-ph].

[21] L. Lehman, Phys. Rev. **D90**, 125023 (2014), arXiv:1410.4193 [hep-ph].

[22] V. Cirigliano, W. Dekens, J. de Vries, M. L. Graesser, and E. Mereghetti, (2017), arXiv:1708.09390 [hep-ph].

[23] S. M. Bilenky and C. Giunti, Int. J. Mod. Phys. **A30**, 1530001 (2015), arXiv:1411.4791 [hep-ph].

[24] S. M. Bilenky and S. T. Petcov, Rev. Mod. Phys. **59**, 671 (1987), [Erratum: Rev. Mod. Phys.60,575(1988)].

[25] J. Engel and J. Menéndez, Reports on Progress in Physics **80**, 046301 (2017).

[26] R. B. Wiringa, V. G. J. Stoks, and R. Schiavilla, Phys. Rev. C **51**, 38 (1995).

[27] S. C. Pieper, AIP Conference Proceedings **1011**, 143 (2008).

[28] C. Patrignani *et al.* (Particle Data Group), Chin. Phys. **C40**, 100001 (2016).

[29] S. Pastore, A. Baroni, J. Carlson, S. Gandolfi, S. C. Pieper, R. Schiavilla, and R. B. Wiringa, (2017), arXiv:1709.03592 [nucl-th].

[30] J. Menendez, private communication.

[31] J. Hyvärinen and J. Suhonen, Phys. Rev. **C91**, 024613 (2015).

[32] J. Carlson, S. Gandolfi, F. Pederiva, S. C. Pieper, R. Schiavilla, K. E. Schmidt, and R. B. Wiringa, Rev. Mod. Phys. **87**, 1067 (2015), and references therein.

[33] J. Carlson and R. Schiavilla, Rev. Mod. Phys. **70**, 743 (1998), and references therein.

[34] S. Bacca and S. Pastore, Journal of Physics G: Nuclear and Particle Physics **41**, 123002, and references therein.

[35] M. L. Graesser, JHEP **08**, 099 (2017), arXiv:1606.04549 [hep-ph].

[36] G. Prezeau, M. Ramsey-Musolf, and P. Vogel, Phys. Rev. **D68**, 034016 (2003), arXiv:hep-ph/0303205 [hep-ph].

[37] V. Cirigliano, W. Dekens, M. Graesser, and E. Mereghetti, Phys. Lett. **B769**, 460 (2017), arXiv:1701.01443 [hep-ph].

[38] S. Weinberg, Phys. Lett. **B251**, 288 (1990).

[39] S. Weinberg, Nucl. Phys. **B363**, 3 (1991).

[40] M. J. Savage, Phys. Rev. **C59**, 2293 (1999), arXiv:nucl-th/9811087 [nucl-th].

[41] J. Menéndez, D. Gazit, and A. Schwenk, Phys. Rev. Lett. **107**, 062501 (2011), arXiv:1103.3622 [nucl-th].

[42] J. Engel, F. Šimkovic, and P. Vogel, Phys. Rev. **C89**,

064308 (2014), arXiv:1403.7860 [nucl-th].

[43] J. Menéndez, in *Prospects in Neutrino Physics (Nu-Phys2015) London, UK, December 16-18, 2015* (2016) arXiv:1605.05059 [hep-ph].

[44] M. Doi, T. Kotani, and E. Takasugi, Prog. Theor. Phys. Suppl. **83**, 1 (1985).

[45] K. Muto, E. Bender, and H. V. Klapdor, Z. Phys. **A334**, 187 (1989).

[46] V. Cirigliano, W. Dekens, E. Mereghetti, and A. Walker-Loud, (2017), arXiv:1710.01729 [hep-ph].

[47] R. B. Wiringa, Phys. Rev. C **43**, 1585 (1991).

[48] B. S. Pudliner, V. R. Pandharipande, J. Carlson, S. C. Pieper, and R. B. Wiringa, Phys. Rev. C **56**, 1720 (1997).

[49] N. Metropolis, A. W. Rosenbluth, M. N. Rosenbluth, A. H. Teller, and E. Teller, The Journal of Chemical Physics **21**, 1087 (1953), http://dx.doi.org/10.1063/1.1699114.

[50] S. C. Pieper and R. B. Wiringa, Ann. Rev. Nucl. Part. Sci. **51**, 53 (2001), arXiv:nucl-th/0103005 [nucl-th].

[51] S. Pastore, S. C. Pieper, R. Schiavilla, and R. Wiringa, Phys. Rev. **C87**, 035503 (2013).

[52] R. B. Wiringa, Phys. Rev. C **73**, 034317 (2006).

[53] M. Piarulli, L. Girlanda, R. Schiavilla, R. N. Pérez, J. E. Amaro, and E. R. Arriola, Phys. Rev. C **91**, 024003 (2015).

[54] J. E. Lynn, J. Carlson, E. Epelbaum, S. Gandolfi, A. Gezerlis, and A. Schwenk, Phys. Rev. Lett. **113**, 192501 (2014), arXiv:1406.2787 [nucl-th].

[55] M. Piarulli *et al.*, (2017), arXiv:1707.02883 [nucl-th].

[56] M. Pervin, S. C. Pieper, and R. B. Wiringa, Phys. Rev. **C76**, 064319 (2007), arXiv:0710.1265 [nucl-th].

[57] S. Pastore, R. B. Wiringa, S. C. Pieper, and R. Schiavilla, Phys. Rev. **C90**, 024321 (2014), arXiv:1406.2343 [nucl-th].

[58] V. M. Datar *et al.*, Phys. Rev. Lett. **111**, 062502 (2013), arXiv:1305.1094 [nucl-ex].

[59] J. Menéndez, N. Hinohara, J. Engel, G. Martínez-Pinedo, and T. R. Rodríguez, Phys. Rev. **C93**, 014305 (2016), arXiv:1510.06824 [nucl-th].

[60] J. Menéndez, T. R. Rodríguez, G. Martínez-Pinedo, and A. Poves, Phys. Rev. **C90**, 024311 (2014), arXiv:1401.0651 [nucl-th].

[61] J. Menéndez, A. Poves, E. Caurier, and F. Nowacki, Nucl. Phys. **A818**, 139 (2009), arXiv:0801.3760 [nucl-th].

[62] J. Barea and F. Iachello, Phys. Rev. **C79**, 044301 (2009).

[63] J. Barea, J. Kotila, and F. Iachello, Phys. Rev. **C91**, 034304 (2015), arXiv:1506.08530 [nucl-th].

[64] D. Shukla, J. Engel, and P. Navratil, Phys. Rev. C **84**, 044316 (2011).

[65] Y. Iwata, N. Shimizu, T. Otsuka, Y. Utsuno, J. Menéndez, M. Honma, and T. Abe, Phys. Rev. Lett. **116**, 112502 (2016), [Erratum: Phys. Rev. Lett.117,no.17,179902(2016)], arXiv:1602.07822 [nucl-th].

[66] F. Šimkovic, A. Faessler, V. Rodin, P. Vogel, and J. Engel, Phys. Rev. C **77**, 045503 (2008).

[67] B. Ananthanarayan and B. Moussallam, JHEP **06**, 047 (2004), arXiv:hep-ph/0405206 [hep-ph].

[68] W. T. Chou, E. K. Warburton, and B. A. Brown, Phys. Rev. **C47**, 163 (1993).

[69] A. Baroni, L. Girlanda, S. Pastore, R. Schiavilla, and M. Viviani, Phys. Rev. **C93**, 015501 (2016), [Erratum: Phys. Rev.C95,no.5,059901(2017)], arXiv:1509.07039 [nucl-th].

[70] H. Krebs, E. Epelbaum, and U.-G. Meiner, Annals of Physics **378**, 317 (2017).